Near-continuously synthesized leading strands in *Escherichia coli* are broken by ribonucleotide excision

Glen E. Cronan[a], Elena A. Kouzminova[a], and Andrei Kuzminov[a,1]

[a]Department of Microbiology, University of Illinois at Urbana–Champaign, Urbana, IL 61801

Edited by Thomas A. Kunkel, National Institute of Environmental Health Sciences, NIH, Research Triangle Park, NC, and accepted by Editorial Board Member Kiyoshi Mizuuchi December 10, 2018 (received for review August 23, 2018)

In vitro, purified replisomes drive model replication forks to synthesize continuous leading strands, even without ligase, supporting the semidiscontinuous model of DNA replication. However, nascent replication intermediates isolated from ligase-deficient *Escherichia coli* comprise only short (on average 1.2-kb) Okazaki fragments. It was long suspected that cells replicate their chromosomal DNA by the semidiscontinuous mode observed in vitro but that, in vivo, the nascent leading strand was artifactually fragmented postsynthesis by excision repair. Here, using high-resolution separation of pulse-labeled replication intermediates coupled with strand-specific hybridization, we show that excision-proficient *E. coli* generates leading-strand intermediates >10-fold longer than lagging-strand Okazaki fragments. Inactivation of DNA-repair activities, including ribonucleotide excision, further increased nascent leading-strand size to ∼80 kb, while lagging-strand Okazaki fragments remained unaffected. We conclude that in vivo, repriming occurs ∼70× less frequently on the leading versus lagging strands, and that DNA replication in *E. coli* is effectively semidiscontinuous.

replication intermediates | Okazaki fragments | the leading strand | ligase mutant | ribonucleotide excision repair

The two strands of a duplex DNA are paired in antiparallel fashion, as first proposed by Watson and Crick (1), perhaps to ensure that optimal base pairing is sequence-independent (2). Early studies on the mechanism of cellular DNA replication revealed that simultaneous replication of both parental strands of chromosomal DNA happens at Y-shaped structures (3, 4) called "replication forks" (5, 6). Contemporaneous in vivo experiments with replication intermediates (7) and in vitro characterization of various DNA polymerases (8–10) showed DNA synthesis only in the 5′→3′ direction, necessitating that in antiparallel DNA duplexes at least one of the strands at the replication fork must be synthesized discontinuously (11).

Indeed, discontinuous DNA replication was discovered by Okazaki and others, using experiments where nascent DNA was pulse-labeled, denatured, and separated by size using alkaline-sucrose (AS) gradients (12–14). Unexpectedly, Okazaki's results showed that all nascent DNA in bacteria is originally synthesized as low molecular weight (LMW) 1- to 2-kb-long replication intermediates (RIs) (11, 13, 15–19), which hybridized to both parental DNA strands (17, 20). Furthermore, pulse–chase experiments confirmed that these initially small fragments were later joined together to form high molecular weight (HMW), chromosome-length DNA strands (12, 18, 19). Fellow researchers coined the term "Okazaki fragments" (21, 22) to describe these LMW RIs, and similar findings of fully discontinuous DNA replication (Fig. 1*A*, *Top*) were promptly confirmed without exception in diverse experimental systems, including mammalian cells (23–25), bacteria (20, 21, 26, 27), and lower eukaryotes (28, 29).

Importantly, due to the rapidity of RI joining in unicellular organisms, isolation of their Okazaki fragments necessitates inhibition of RI maturation (joining) activities. In bacteria, LMW RIs (Okazaki fragments) mature into full-length DNA strands by a two-enzyme system, composed of a repair DNA polymerase (DNA pol I, g*ppolA*) and DNA ligase (g*pligA*). Polymerase I removes the RNA primer of the downstream fragment while simultaneously extending the current fragment, thus generating an all-DNA nick, which is then closed by DNA ligase (8). This maturation process ensures that inactivation of DNA ligase preserves Okazaki fragments (albeit lacking their RNA primers), as first reported by Okazaki himself (13, 18). In fact, no chromosomal-size HMW RIs have ever been observed in ligase-minus conditions (21, 26, 28–34).

However, inactivation of ligase also prevents joining of nicks arising from excision-repair processes. Replicative DNA polymerases readily incorporate various base analogs such as hypoxanthine into the growing chain, from where they are quickly removed by specialized excision enzymes (35, 36). Incorporation–excision reactions of this type may fragment the nascent DNA, with the resulting shorter pieces appearing similar in size to true RNA-primed Okazaki fragments (Fig. 1*A*). This potential for excision-driven formation of LMW RIs was confirmed for uracil-DNA incorporation using *Escherichia coli dut* mutants that, due to the defective dUTPase, frequently incorporate dU into their nascent DNA (37, 38). This coupling of incorporation and fragmentation was further characterized using *dut* and *ung* mutants (deficient in DNA-uracil excision) in a cell-free system (39, 40), and subsequently in *thyA* mutant *Bacillus subtilis* (which synthesized only LMW RIs), where a dramatic increase in RI size was noticed after inactivation of uracil excision (41). However, a *thyA* mutant of *E. coli* synthesized mostly HMW DNA, which was unaffected by *ung* inactivation (42). Importantly, the *ung* mutant

Significance

The antiparallel orientation of strands in a DNA duplex and unidirectional polarity of DNA polymerases necessitate that replication forks operate semidiscontinuously. That is, the strand replicated codirectionally to replication-fork movement, termed the "leading" strand, is synthesized continuously, while the oppositely oriented "lagging" strand is synthesized in short "Okazaki" fragments, later joined by ligase. Semidiscontinuous replication is observed in vitro, even in reactions lacking ligase. However, in vivo, in ligase (*lig*) mutants, nascent DNA from both strands is found only in small pieces. Here, we report the continuous synthesis of leading strands in *lig* mutant *Escherichia coli* lacking all DNA excision-repair activities and, using an improved sucrose-gradient system, identify misincorporated ribonucleotides as the major driver of leading-strand fragmentation.

Author contributions: G.E.C., E.A.K., and A.K. designed research; G.E.C. and E.A.K. performed research; G.E.C., E.A.K., and A.K. analyzed data; and G.E.C. and A.K. wrote the paper.

The authors declare no conflict of interest.

This article is a PNAS Direct Submission. T.A.K. is a guest editor invited by the Editorial Board.

[1]To whom correspondence should be addressed. Email: kuzminov@illinois.edu.

This article contains supporting information online at www.pnas.org/lookup/suppl/doi:10.1073/pnas.1814512116/-/DCSupplemental.

Published online January 7, 2019.

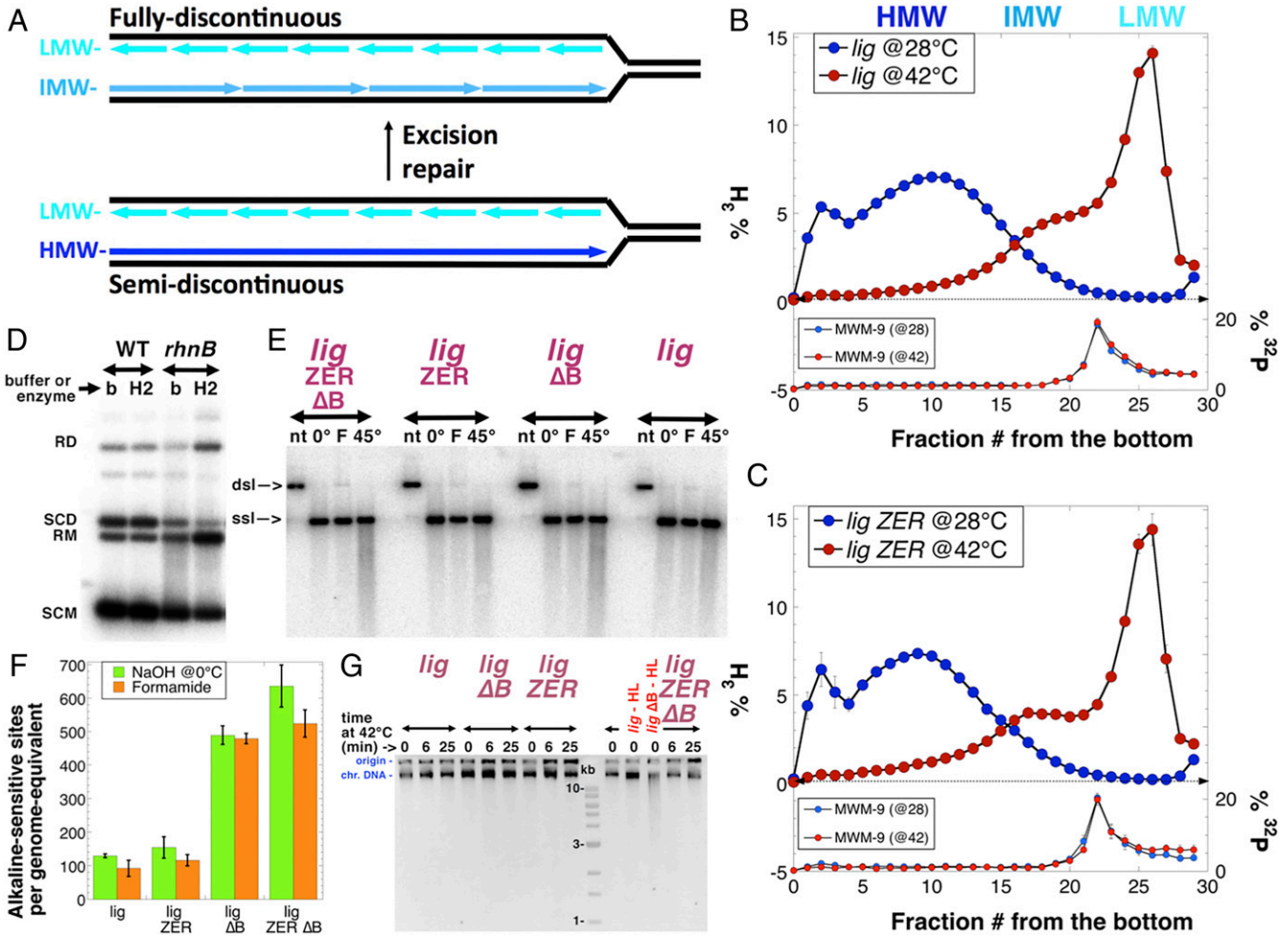

Fig. 1. Continuously synthesized leading strand may appear discontinuous due to excision repair. (*A*) A scheme of fully discontinuous and semidiscontinuous replication highlighting the possible effects of excision repair. (*B*) Analysis by high-resolution alkaline-sucrose gradient of ligase-deficient replication intermediates reveals a substantial shoulder population of higher molecular weight intermediates. Here and henceforth, all gradients are sedimented from right (*Top*) to left (*Bottom*), with HMW species on the left, and LMW species on the right. The main panel shows the distribution of the [^{3}H]dT pulse-labeled replication intermediates (red; at 42 °C for 2 min) or chronically labeled total chromosomal DNA (blue; at 28 °C for 35 min). (*B*, *Bottom*) The position of ^{32}P-labeled molecular weight markers of the individual gradients (typically MWM-9, which is a 9.3-kb PCR fragment), color matched to the main panel. Specifically, for this panel, the strain is *lig* (GR501). The values are means ± SEM of 31 to 44 independent repetitions. Due to the significant number of repetitions, most error bars are completely masked by the symbols. (*C*) Same as in *B*, but the strain is *lig ZER* (LA111, the excision-minus GR501). The values are means ± SEM of four to nine independent repetitions. (*D*) The *rnhB* mutants accumulate significant density of single rNs in their DNA, as measured by supercoiled plasmid relaxation with RNase HII in vitro. RD, relaxed dimer; RM, relaxed monomer; SCD, supercoiled dimer; SCM, supercoiled monomer. Strains: WT, AB1157; *rnhB*, L-415. (*E*) Accumulation of alkaline-sensitive material in the DNA of excision-minus, *rnhB*, or combined mutants. Unlike in *D*, plasmid DNA was linearized with MluI and then treated as follows: nt, no treatment; 0°, 0.2 M NaOH, 0 °C × 5 min (background #1); F, 100% formamide, 37 °C × 5 min (background #2); 45°, 0.3 M NaOH, 45 °C × 90 min. Plasmid species: dsl, double-strand linear; ssl, single-strand linear. Strains: *lig*, GR501; *lig ZER*, LA111; *lig ΔB* (GR501 Δ*rnhB*), eGC193; *lig ZER ΔB*, eGC197. (*F*) The density of alkaline-sensitive sites was determined from several gels such as in *E* and is presented as the number per genome equivalent (±SEM). (*G*) Neutral 0.8% agarose gel separation of the chromosomal DNA prepared in agarose plugs and denatured in 0.2 M NaOH at 0 °C for 30 min to reveal any ss breaks. An inverted ethidium bromide (EtBr)-stained image is shown. As a positive control for ss-break detection, we incubated the two control lanes, marked HL, in 0.3 M NaOH at 45 °C for 90 min to quantitatively hydrolyze single DNA-rNs; this nicks on average every 10 kb of the DNA strands of the *lig* ΔB mutant; the *lig* DNA remains intact. Strains are like in *E*.

E. coli continued to synthesize exclusively LMW RIs under maturation-deficient conditions (30, 34, 43), indicating that uracil excision was not a source of nascent leading-strand fragmentation.

That the leading strand could be synthesized by a continuous mechanism in the complete absence of ligase was amply demonstrated in various in vitro replication systems using highly purified replisomes (44–46). The resulting semidiscontinuous DNA-replication model (Fig. 1*A*, *Bottom*) became a fixture of textbooks (47), even though it contradicted the bulk of in vivo results, and persisted despite our lack of understanding of the supposed fragmenting activities (22). Several attempts to identify the in vivo DNA-repair activities responsible for the putative postsynthesis fragmentation in *E. coli* were unsuccessful (30, 33, 34). The most recent study went so far as to inactivate all eight individual DNA glycosylases (eliminating base-excision repair), in addition to blocking nucleotide-excision repair (*uvrA*), mismatch removal (*mutS*), and alternative excision repair (*nfi*), yet even this dodecuple mutant [including the *ligA251*(Ts) defect] showed no increase in RI size (31). Still, those authors were aware of the possibility that the tails of intermediate molecular weight (IMW) species could represent the leading-strand RIs (31). Besides, other work showed that only ∼50% of Okazaki fragments from wild-type *E. coli* harbored the 5′-RNA moiety indicative of priming, suggesting that the other half was generated by excision (48).

Two recent developments prompted our reevaluation of this conundrum. First, development of a higher-resolution AS-gradient system, buttressed by MW markers from 1 to 170 kb, revealed a distinct IMW (5- to 25-kb) shoulder adjoining the main LMW (~1.2-kb) Okazaki fragment peak formed under ligase-deficient (*lig*) conditions (Fig. 1*B*). Furthermore, the excision mutant used in previous work, deficient in all DNA-only excision-repair systems (now called *lig ZER*; zero excision repair), that previously produced exactly the same RI distribution as excision-proficient cells in regular AS gradients (31), now developed a clear separation of the two RI peaks in the improved AS-gradient system (Fig. 1*C*). Thus, this high-resolution analysis confirmed the presence of two distinct RI populations of significantly different molecular weight. Second, a new DNA contaminant was identified: Monoribonucleotides (rNs) were found to misincorporate into the chromosomal DNA of eukaryotes at high frequency (49, 50), even though in *B. subtilis* the density of a single DNA-rN misincorporation initially appeared qualitatively low (51). Recently, the density of single DNA-rNs in the *rnhB* mutant *E. coli* was found to be one in 14,000 nt (52) (Fig. 1*D*). As DNA-rNs are efficiently excised (52), one chain break per 14,000 nt in the leading strand could produce fragments similar in size to the observed IMW fragments (Fig. 1 *B* and *C*). Unexpectedly, this significant accumulation of DNA-rNs was without any effect in *E. coli*, as *rnhB* mutants showed essentially wild-type behavior (52).

To test DNA-rNs as a potential source of RI breakage, we added an *rnhB* defect in ribonucleotide excision repair to our *lig ZER* strain (31). The resulting *lig ZER ΔB* mutant, in addition to the *ligA251* temperature-sensitive ligase deficiency, carries 12 additional mutations completely inactivating all known excision-repair pathways in *E. coli*, including ribonucleotide-excision repair. By preventing the excision of all known "incorrect" bases, we hoped to increase the stability of nascent DNA and preserve the true size of RIs for examination. However, AS gradients appeared chemically inadequate for the task of separating the ribonucleotide-containing RIs from *rnhB* mutants, as the strongly basic pH of AS gradients, required to denature RIs from their template strands, efficiently hydrolyzes mono-rNs in DNA (52) and also destabilizes abasic sites (53). Therefore, we developed a pH-neutral denaturing gradient system to separate RIs without inducing breakage at alkaline-sensitive sites. Employing this gradient system, in concert with traditional alkaline-sucrose methods and strand-specific hybridization of DNA from gradient fractions, we demonstrate that the *lig ZER ΔB* mutant of *E. coli* replicates its leading strand by an essentially continuous mechanism.

Results

The Density of Alkaline-Sensitive Sites in Nascent DNA. Our basic protocol for RI detection follows the classic outline (15) and includes shifting exponentially growing cultures of *ligA251*(Ts) mutant strains from 28 to 42 °C for 4 min to inactivate DNA ligase, followed by addition of a [^{3}H]thymidine label, and continuing incubation at 42 °C for 2 additional minutes to label RIs. Following RI labeling, cellular metabolism is stopped instantly, the cells are lysed to release their genomic DNA, and the DNA is then purified and sedimented on alkaline-sucrose gradients. We never exceeded 6 min as the total incubation time of the *ligA251* (Ts) mutant at 42 °C, avoiding chromosome fragmentation that begins after 20 min at the nonpermissive temperatures in this mutant (54) (*SI Appendix*, Fig. S1). The basic pH of alkaline sucrose denatures labeled RIs, freeing them from the unlabeled template strands, so they can sediment as single-stranded DNAs to be separated according to their length (molecular weight) (15). Importantly, the same alkaline pH at 0°C treatment of the chromosomal DNA of all our experimental strains [all *ligA*(Ts) mutants] after incubation at 42 °C for up to 25 min reveals no accumulation of single-strand breaks in bulk genomic DNA (Fig. 1*G* and *SI Appendix*, Fig. S1).

In this work, resolution of AS gradients was optimized, particularly for the IMW size range of 5 to 50 kb, by two modifications to the previous methodology: (*i*) The significantly reduced total applied g force maintained the majority of chromosomal DNA within the gradient instead of sedimenting it into the cushion at the bottom of the tube; and (*ii*) the apparatuses used for the pouring and fractionation of gradients were completely reworked (*Material and Methods*). A 9.3-kb ^{32}P-labeled DNA was included in every gradient, as both an MW marker and positional control (Fig. 1 *B* and *C*, *Bottom*). In some experiments, virion DNAs from phages lambda (48.5 kb) and T4D (~170 kb) were also used as, correspondingly, IMW and HMW marker DNAs, and to build an MW standard curve (*SI Appendix*, Fig. S5) (55). Additionally, the MW marker DNAs served as internal controls against nonspecific DNA hydrolysis.

As stated in the Introduction, it became apparent that our previous conclusions concerning LMW RIs in the *ligA251* mutant at 42 °C (30, 31) should be revisited, as the IMW shoulder in the RI distribution of the excision+ *lig* strain clearly shifted to higher molecular weight in the *lig ZER* mutant (Fig. 1*B* versus Fig. 1*C*, compare fractions 16 to 21; for quantification, see *SI Appendix*, Fig. S5*D*). Meanwhile, in vitro plasmid relaxation by RNase HII indicated a significant density of single ribonucleotides in the DNA of *rnhB* mutants (Fig. 1*D*) (52). Since for this project it was more relevant to assess the density of alkaline-sensitive sites in DNA, we treated linearized plasmid DNA with alkali (0.3 M NaOH, 90 min at 45 °C), analyzing the intactness of the strands in neutral agarose gels (Fig. 1*E*). We found alkaline-induced nick densities in the *lig ΔB* and *lig ZER ΔB* mutants of one per 8,000 to 9,000 nt, translating into 500 to 600 alkaline-sensitive sites per genome equivalent (Fig. 1 *E* and *F*). The increase of alkaline-sensitive sites in the DNA of the *lig ZER* mutant compared with the *lig* mutant (both strains RnhB+) was insignificant (Fig. 1 *E* and *F*). Therefore, the density of DNA-rNs in the *rnhB* mutants pointed to ribonucleotides as the major genome contaminant, suggesting that in AS gradients, alkaline hydrolysis of DNA-rNs masks the true size of RIs. This prompted us to develop a pH-neutral denaturing sucrose-gradient system for separation of rN-containing DNA.

Formamide-Urea Gradients Reveal HMW Replication Intermediates. Formamide and urea are known to destabilize duplex DNA without breaking strands at rNs or other modified bases (56–58). In fact, formamide-sucrose gradients were used before to separate RIs, to avoid the instability of potential abasic sites in alkali (33) and to preserve RNA-primed lagging strands (59). After experimentation with various concentrations of formamide, urea, and sucrose, we settled on gradients of 5 to 40% sucrose in 70% formamide and 1 M urea, with sample loading in 50% formamide and ~5 M urea. In these formamide-urea-sucrose (FUS) gradients, the sedimentation patterns of HMW chromosomal DNA (ligase+ conditions), or LMW RIs (ligase– conditions), were similar to those obtained in AS gradients (Fig. 2*A*). Besides the almost coincidental positions of major peaks, a significant shoulder of IMW RIs can clearly be seen in both systems. Similar to AS gradients, the distribution of IMW RIs from the *lig ZER* strain shifts to higher molecular weights and develops into a separate peak in FUS gradients (Fig. 2*B*), confirming that longer RIs are fragmented into shorter ones by excision repair in nascent DNA of WT cells.

Most importantly, FUS gradients allowed us to experiment with the *rnhB* mutants without inducing artifactual rN hydrolysis. As expected, we found that inactivation of RNase HII in the original *ligA* mutant shifted IMW RIs even further toward HMWs (Fig. 2*B*, *lig ΔB* @42 °C), showing that "contamination" of nascent DNA by ribonucleotides exceeded contamination by

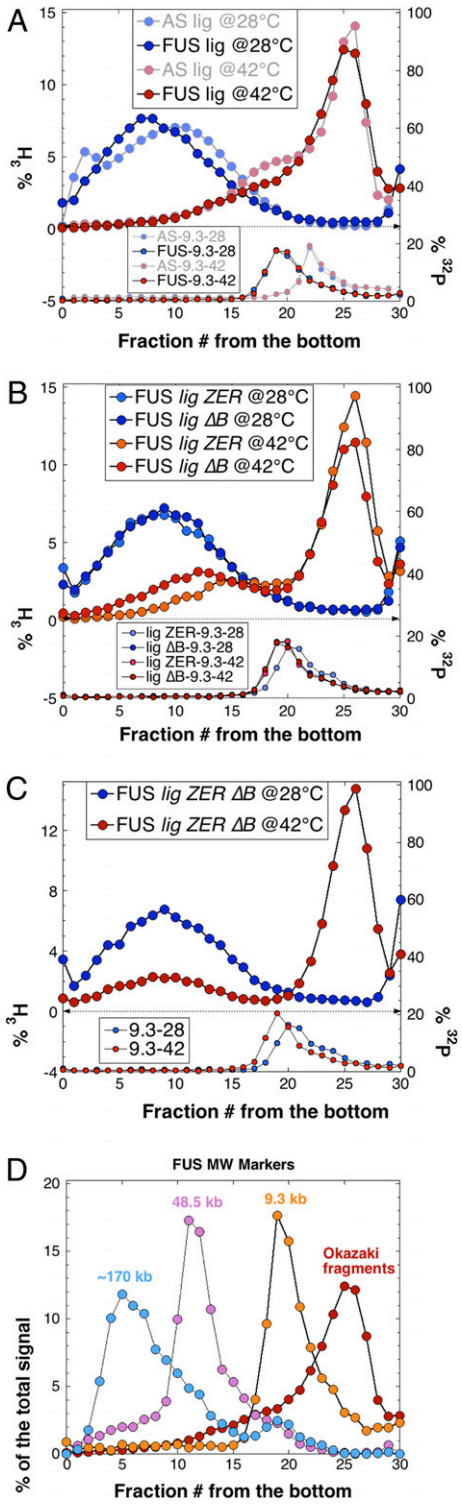

Fig. 2. Formamide-urea-sucrose gradients reveal HMW replication intermediates in the *lig ZER ΔB* mutant. (*A*) The separation pattern of FUS gradients for the *lig* mutant (GR501). The temperature of [^{3}H]dT labeling is indicated. The corresponding alkaline-sucrose gradients from Fig. 1*B* are shown in faded colors for comparison. (*B*) The effect of removal of DNA-rN excision (*lig ΔB*) versus all other excision-repair systems (*lig ZER*) in FUS gradients. Strains: *lig ZER*, LA111; *lig ΔB*, eGC193. (*C*) The effect of the removal of both DNA-rN excision and all other excision-repair systems in one strain (*lig ZER ΔB*, eGC197) in FUS gradients. (*D*) FUS-gradient separation of our standard molecular weight markers: the 9.3-kb PCR fragment, phage lambda (48.5 kb), and phage T4 (~170 kb), relative to the Okazaki fragments peak (~1.1 kb) from the *lig* mutant (GR501).

all other DNA modifications removed by all-DNA excision-repair systems inactivated in the *lig ZER* mutant. A crucial finding came from introduction of the *rnhB* defect into the *lig ZER* strain, to yield the *lig ZER ΔB* mutant deficient in all known initiators of excision repair in *E. coli*. In the FUS gradients, RIs from the *lig ZER ΔB* strain form two well-separated peaks: the standard LMW peak of Okazaki fragments and a now fully separate HMW peak similar in size to the chronically labeled chromosome (Fig. 2*C*). Importantly, in all these mutants (Fig. 2; also, the four gradients are overlaid in Fig. 3*B*), while the IMW peak gradually becomes HMW, the LMW peak does not shift to higher molecular weights, confirming that it is insensitive to repair activities and therefore likely represents true Okazaki fragments.

The MW standards for FUS gradients show a uniform separation between Okazaki fragments (1.2 kb), the 9.3-kb PCR fragment, lambda chromosome (48.5 kb), and T4 chromosome (~170 kb) (Fig. 2*D*). This allowed us to estimate the size of the HMW RI peak as stretching from ~20 kb to 300 kb, with the major fraction found between 50 and 150 kb (Fig. 2 *C* and *D*; also see *SI Appendix*, Figs. S4 and S5). We conclude that when all known excision-repair activities are eliminated (in the *lig ZER ΔB* mutant), and alkaline hydrolysis of DNA-rNs is prevented (in FUS gradients), RI distribution becomes strictly bimodal, with the HMW fraction appearing to result from continuous synthesis.

Return to Alkaline-Sucrose Gradients Facilitates Testing Strand Identity of RIs. Continuous synthesis of half of the RIs is consistent with the semidiscontinuous model of the replication fork (Fig. 1*A*), which makes a strong prediction about strand identity: According to the semidiscontinuous model, LMW RIs represent the lagging strand, whereas HMW RIs come from the leading strand. In previous studies, LMW RIs from maturation-deficient (both excision-proficient and -deficient) mutants hybridized equally to both strands (17, 20, 27, 31, 33, 60). Unique replication origin and terminus of bacterial chromosomes (61), by ensuring a fixed direction of movement of replication forks through specific loci, facilitate unequivocal determination of the leading versus lagging source of RIs. Would hybridization of *lig ZER ΔB* mutant RIs reveal a mixture of leading and lagging strands within each peak or their partitioning between the two peaks?

To answer this question, we sought to isolate different populations of RIs directly from gradient fractions and to query their strand identity by strand-specific hybridization. In so doing, technical considerations forced us to return to the alkaline-gradient system, which is more rapid, taking 1 d of centrifugation instead of 2 for FUS gradients, and whose lower viscosity greatly increased the speed with which fractions could be centrifugally dialyzed. We managed to dramatically reduce the problem of DNA-rN hydrolysis in alkaline pH due to our previous serendipitous finding that rN-containing DNA oligos become stable at alkaline pH if kept on ice (ref. 52; Fig. 1*E*, lanes 0° for *lig ZER ΔB* and *lig ΔB* strains). As a proof of concept, rRNA stability in 0.2 M NaOH was greatly increased at 0 °C, compared with 16 °C and especially 37 °C (Fig. 3*A*, lines c to e), while the same material incubated in the FUS loading buffer was stable at all temperatures (Fig. 3*A*, lines k to m). Calculations of the rate of hydrolysis of rRNA at 0 °C (*SI Appendix*, section 10) show that a similarly slow hydrolysis of sparse DNA-rNs should have only a minor effect on the final size of the HMW distribution.

We estimated the degree of alkaline hydrolysis in AS(4 °C) gradients using the DNA species most sensitive to breakage, the HMW (chromosomal) DNA. Separation of chromosomal DNAs from the RnhB+ strain (*lig*) and its *rnhB* mutant sibling (*lig ΔB*) that accumulate DNA-rNs in AS(4 °C) gradients revealed a difference of two fractions between the peaks of HMW material (Fig. 3*C*), consistent with a minor instability of single DNA-rNs under these conditions. Subsequent experiments confirmed these

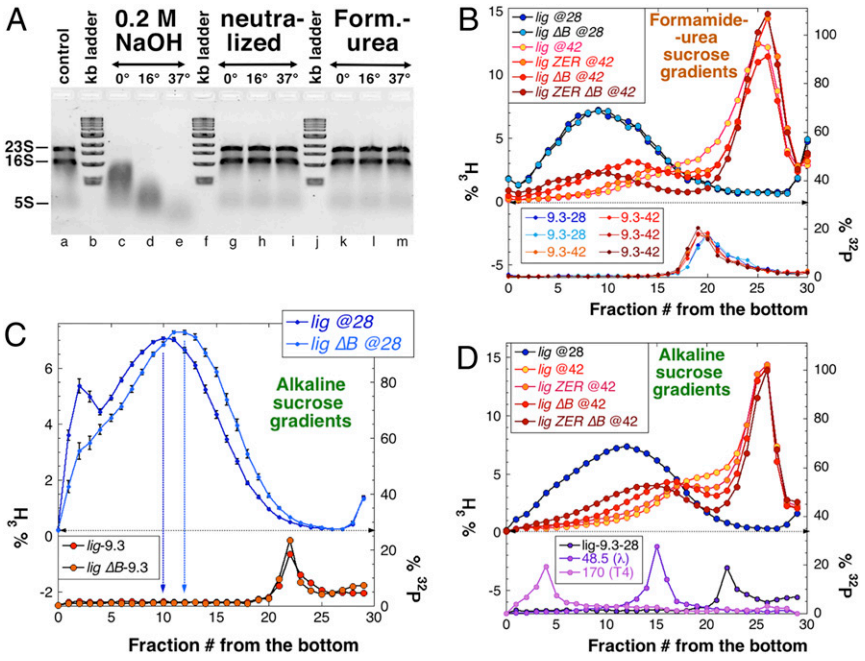

Fig. 3. Alkaline-sucrose gradients, sedimented at 4 °C, detect HMW replication intermediates. (*A*) The relative stability of RNA in alkaline solution at 0 °C. Incubation was for 15 min in the indicated conditions (either 0.2 M NaOH, preneutralized 0.2 M NaOH, or formamide-urea loading buffer), at the indicated temperatures (either 0, 16, or 37 °C). Control, input total *E. coli* RNA (mostly 23S+16S+5S rRNA). The reversed image of EtBr-stained 1.2% agarose gel is shown, to visualize the kilobase ladder. (*B*) The FUS-gradient separation of replication intermediates from the four ligase-deficient mutants with increasing levels of excision-repair deficiency. Strains: *lig*, GR501; *lig ΔB*, eGC193; *lig ZER*, LA111; *lig ZER ΔB*, eGC197. (*C*) When sedimented through chilled AS gradients, genomic DNA from the *rnhB* mutant displays a reduced size in comparison with WT, presumably due to limited alkaline hydrolysis of DNA-rNs. Vertical arrows indicating peak fractions are color matched to the corresponding gradients. Mean ± SEM for multiple experiments [*lig* (GR501) $n = 44$; *lig ΔB* (eGC193) $n = 10$]. (*D*) As in *B*, but AS gradients at 4 °C. Each curve represents the mean of between 7 and 45 separate experiments; error bars are omitted for clarity. The visible shift to the right of the HMW peaks compared with the FUS gradients in *B* is ostensibly due to DNA-rN hydrolysis.

predictions in ligase-minus conditions. If DNA-rNs were significantly hydrolyzed during AS-gradient centrifugation at 4 °C, the distribution of RIs from the *lig ΔB* mutant would sediment similar to those from its *lig* (RnhB+) parent. This is clearly not the case. Comparison of the four RI profiles from the FUS gradients (Fig. 3*B*), with identical material sedimented through AS gradients at 4 °C (Fig. 3*D*), clearly demonstrates conservation of the relative sedimentation patterns between the two systems. In particular, a large gap between the HMW and LMW species of RIs from the *lig ZER ΔB* mutant was essentially unchanged in AS gradients (Fig. 3*D*), allowing for a clean isolation of the two molecular weight populations with minimal cross-contamination.

Strand-Specific Hybridization of Tritiated RIs. To query the strand identity of HMW versus LMW RIs, we pooled three distinct populations of labeled DNAs from AS(4 °C) gradients (Fig. 4*A*) for hybridization. The pooled fractions were concentrated to a small volume by centrifugal dialysis, sonicated (*SI Appendix*, Fig. S6), and split in half for hybridization with one of the two complementary strand-specific ssRNAs. The sonication step was important to reduce solution viscosity and to minimize "sandwich hybridization" (62) (*SI Appendix*, Fig. S8).

The strand-specific ssRNAs used as hybridization targets were generated by in vitro T7 transcription of an 8.8-kb genomic fragment containing the *gspD-M* operon. The *gsp* operon, located at position 3456 to 3465 kbp on the *E. coli* chromosome, was chosen for its distance from *oriC* (~500 kbp), transcriptional silence (63), and relative lack of predicted secondary structures. ssRNAs produced in these in vitro reactions were cross-linked to nylon membranes in quantities sufficient to prevent saturation of probe binding (*SI Appendix*, Fig. S7) and tested for strand specificity in model hybridization reactions using ^{32}P end-labeled ssDNA oligo probes (*SI Appendix*, Fig. S8*A*). Input control DNA containing equal amounts of tritiated Watson and Crick strands was obtained from pooled fractions 5 to 13 (60 to 150 kb) of DNA labeled for 35 min at 28 °C (LigA$^+$ conditions). As expected, this chronically labeled genomic DNA hybridized equally well to either strand, yielding a lead/lag ratio close to unity (Fig. 4*A*, *Left* pie chart). To assay RIs formed under *ligA*-deficient conditions, we labeled the *lig* mutant for 2 min at 42 °C and, following sedimentation, separately pooled the HMW/IMW RIs from fractions 8 to 20 (20 to 100 kb), while the LMW RIs were pooled from fractions 23 to 27 (0.5 to 7 kb). In contrast to the hybridization ratio obtained from the chronically labeled chromosomal DNA, the lead/lag ratio for the HMW RIs was 2.81 (*Middle* pie chart in Fig. 4*A*), while the lead/lag ratio for LMW RIs was 0.31 (*Right* pie chart in Fig. 4*A*). In other words, even under excision-proficient conditions where separation between LMW and HMW RIs was minimal, there was a ninefold difference (2.81/0.31) in the strand preference between the two pools of RIs.

When we repeated the strand-specific hybridizations with the same two pools of fractions from the *lig ZER ΔB* strain, in which HMW RIs were clearly separated from the LMW RIs (Fig. 4*B*), we observed a dramatic increase in strand specificity. For this strain, the lead/lag ratio reached 7.33 for HMW RIs (*Left* pie chart in Fig. 4*B*), while decreasing to 0.095 for the LMW RI population (*Right* pie chart in Fig. 4*B*). This 77-fold difference (7.33/0.095) in strand preference between RI pools from the *lig ZER ΔB* mutant reflects a mostly leading-strand origin for HMW RIs, and a mostly lagging-strand origin for LMW RIs. The actual purity of the leading- and lagging-strand fractions should be even higher, as it is compromised by the alkaline hydrolysis of DNA-rNs (Fig. 3*C*) and sandwich hybridization (*SI Appendix*, Fig. S8).

Reversing the Replication Direction Through the Hybridization Region. To test whether the observed lead/lag ratios were truly a reflection of the direction of replication-fork progress through the hybridization region, rather than some intrinsic property of the region itself, we reversed the direction of replication-fork progression through the *gsp* locus. The *ligA251*(Ts) and *rnhB* mutations were moved into the Hfr KL-16 strain (64), in which an integrated F plasmid contributes its active *oriF* ~500 kbp downstream of *gsp*. We then deleted *oriC* in the resulting strain, making chromosomal replication completely dependent on *oriF* (Fig. 5*A*). If, in the original *oriC*-driven strains, the lagging strand at *gsp* was Watson, while the leading strand was Crick, in the *oriF*-driven strain the lagging strand at *gsp* became Crick, while the leading strand became Watson (Fig. 5*A*).

To test this, DNA from the *lig ΔB oriF* Δ*oriC* strain was sedimented and hybridized exactly as for the *oriC*-driven strains. As expected, positionally shifting the chromosomal origin of

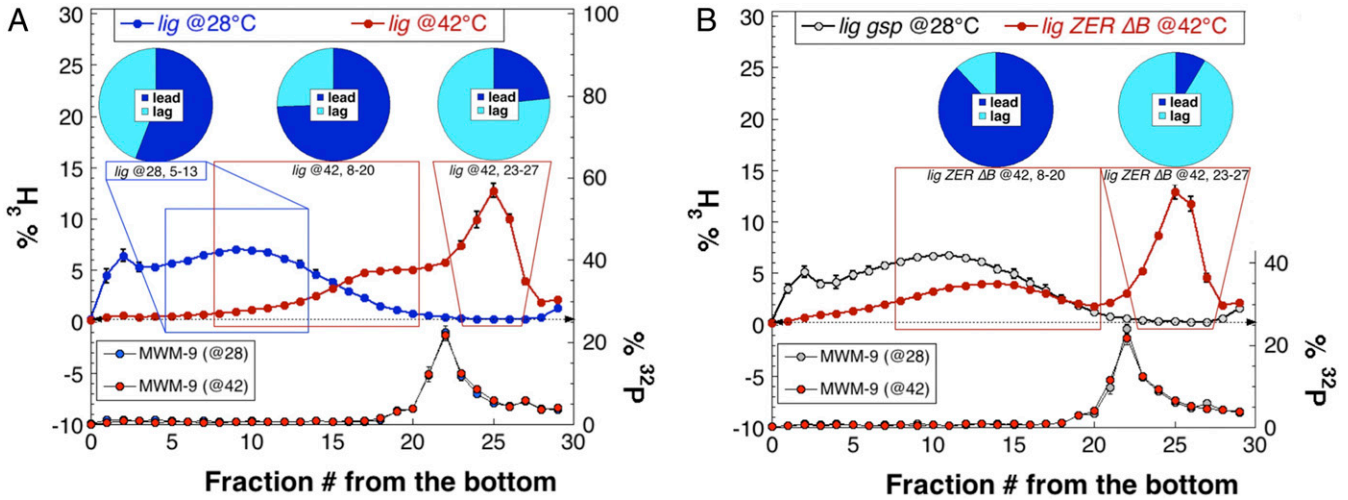

Fig. 4. Strand-specific hybridization of the HMW versus LMW replication intermediates. Strand-specific hybridizations were performed on tritiated DNA isolated directly from alkaline sucrose-gradient fractions. Portions of all gradient fractions were counted to generate the gradient profiles, while the remainder of selected fractions (colored rectangles) were pooled and hybridized against complementary strand-specific ssRNA targets. The specificity (lead/lag) ratios found in the hybridization experiments are shown as pie charts (*Top*), above the corresponding boxes indicating the pooled fractions used for hybridization. Results are shown as the mean of three independent experiments; error bars represent SEM (see Fig. 5*C* for hybridization SEMs; nonnormalized hybridization data are presented in *SI Appendix*, Fig. S9). (*A*) Excision repair-proficient strain *lig* (GR501) was labeled with tritiated thymidine either at 28 °C for 35 min (bulk genomic DNA, blue curve) or 42 °C for 2 min (replication intermediates, red curve). Fractions 5 to 13 from the 28 °C gradient were hybridized to generate the specificity ratio shown in the *Left* pie chart, while fractions 8 to 20 and 23 to 27 from the 42 °C labeling were hybridized to produce the *Center* and *Right* pie charts, respectively. (*B*) As in *A*, but the excision repair-deficient strain *lig ZER ΔB* (eGC197) was labeled at 42 °C for 2 min, and the resulting replication intermediates were pooled from gradient fractions 8 to 20 and 23 to 27 and hybridized to produce the strand-specificity pie charts (shown, correspondingly, *Center* and *Right*).

replication neither influenced the 1:1 hybridization ratio for the control ligase-proficient conditions (Fig. 5*B*, *Left* pie chart), nor did it alter the bimodal nature of the ligase-deficient RI distribution (Fig. 5*B*, red ^{3}H profile). However, 42 °C RI profiles from the *oriF* strain did display an altered ratio of areas under the HMW and LMW RI curves, with ∼70% of total RIs now found under the HMW peak (Fig. 5*B*). The reason for this altered proportion of label in the HMW peak is unknown, but we suspect residual activity of the LigA251(Ts) enzyme at 42 °C in this background, possibly reflecting strain-specific variations in the protein-degradation levels (65, 66).

Nevertheless, the *oriF* strains produced broadly similar hybridization results to those obtained for the *oriC* strains. The lead/lag ratio was 3.1 for the HMW RIs (*Middle* pie chart in Fig. 5*B*), while it was 0.1 for LMW RIs (*Right* pie chart in Fig. 5*B*), yielding a more than 30-fold difference in the relative strand preference between the two pools of RIs. When hybridization results from the *oriC* and *oriF* strains were plotted side by side, the chronically labeled DNA showed an even distribution of label between the two strands, regardless of the replication origin tested (Fig. 5*C*, gray bars). Importantly, shifting the origin of replication relative to the hybridization region reversed the ratios for pulse-labeled fractions: If, in the *oriC* strain, the Watson strand signal was low in a particular MW pool, in the *oriF* strain that pool showed increased signal, and vice versa (Fig. 5*C*), confirming the theoretical considerations (Fig. 5*A*). We conclude that, for at least the *gsp* locus of the chromosome, the leading strands are synthesized as HMW species, while the lagging strands are synthesized as LMW species (Okazaki fragments), independent of the direction of replication.

Periodic Repriming of the Leading Strand. Are the nascent leading strands truly continuous with the rest of the chromosome, or are they periodically reprimed? To detect LMW RIs, the Okazaki group pulse-labeled growing cells with [^{3}H]dT for several seconds (11, 19). They later found that, under ligase-deficient conditions, even with increased pulse length, LMW RIs continued accumulating linearly over at least 1 min without significant increase in length (18). In our hands, with the *ligA251*(Ts) mutant, incubation at 42 °C up to 3 min did not change the overall RI distribution (31). To maximize the yield of material for hybridization, we typically labeled our lig mutants at 42 °C for 2 min. Under this long period of labeling, HMW RIs from the ZER mutant appeared similar in length to the chromosomal DNA (Fig. 3 *B* and *D*), as would be expected if the leading strands were synthesized continuously, without periodic repriming, and therefore were contiguous with the rest of the chromosome (Fig. 6*A*, *Left*) (within the ∼100-kb size limit of intact DNA strands due to our cell-lysis procedure; *SI Appendix*, Fig. S2). At the same time, incubation at 42 °C for 2 min allowed for polymerization of 120 to 150 kb of nascent DNA (54), making it possible that this long pulse time could obscure periodic repriming events (Fig. 6*A*, *Right*).

To detect possible periodic repriming on the leading strand, we labeled the *lig ZER ΔB* mutant under ligase-deficient conditions for times between 10 and 270 s. Since this experiment is exquisitely sensitive to any traces of remaining ligase activity, the *lig ZER ΔB* mutant was labeled at an elevated temperature of 45 °C, 3 °C above normal (but similar results were also obtained at 42 °C). There is little to no active ligase present in these cells, as can be seen from the labeling-time insensitivity of the position and height of the Okazaki fragment peak (Fig. 6*B*). While the Okazaki (LMW) peak remained unchanged, increased labeling time caused the position of the (very broad) leading-strand distribution to shift toward higher molecular weights, while the trough between the two distributions deepened (Fig. 6*B*). Specifically, the leading-strand distribution was centered at ∼20 kb following a 10-s pulse of [^{3}H]dT, but shifted to ∼50 kb following 270 s of labeling. This result is consistent with the periodic repriming of the leading strand, at least every ∼50 kb, although this value is likely an underestimate due to the limited hydrolysis of rNs in alkaline sucrose (Fig. 3 *C* and *D*).

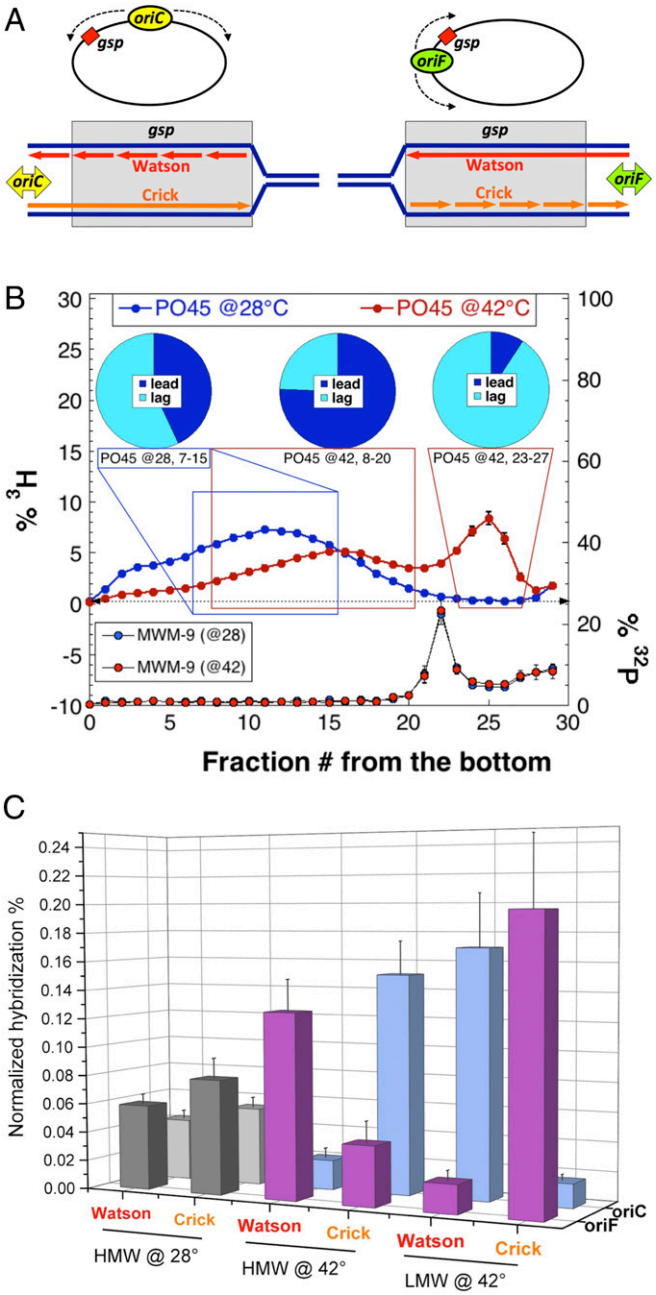

Fig. 5. HMW or LMW character of the RIs in Watson or Crick strands depends on the direction of DNA replication through the hybridization region. (*A*) The relative position of the *gsp* locus versus *oriC* on the chromosome (*Top Left*) ensures that the lagging nascent strand (LMW) is Watson, while the leading nascent strand (HMW) is Crick. The question is: If we switch the direction of the replication fork through the *gsp* region by using *oriF* (*Top Right*), will it make the nascent Watson strand HMW while the nascent Crick strand LMW? (*B*) Strand-specific hybridization of the HMW versus LMW replication intermediates in the *oriF*-driven strain. The strain PO45 is *ligA251*(Ts) Δ*rnhB oriF*+ Δ*oriC* (eGC225). (*B*, *Left*) The pie chart shows the relative leading-strand (blue) and lagging-strand (cyan) components of bulk chromosomal DNA isolated from the *oriF*-driven strain labeled at 28 °C (Lig+ conditions) (fractions 5 to 13 of the blue gradient). The other two pie charts display the strand bias for RIs isolated from fractions 8 to 20 (*Middle*) and 23 to 27 (*Right*), from the same *oriF*-driven strain labeled at 42 °C. (*C*) Summary hybridization data for Watson and Crick strand specificities of bulk chromosomal DNA (28 °C; gray bars) and RIs (42 °C), as assayed at the *gsp* locus, for the *lig ZER ΔB* mutant (eGC197) replicated from *oriC* (back row, light blue) versus PO45 (eGC225) replicated from *oriF* (front row, light purple). The *oriC*-driven strain hybridization data are from Fig. 4*B*, while the *oriF*-driven strain data are from *B*. Data are the mean ± SEM, $n = 3$ for all cases.

Discussion

The results presented here largely resolve one of the oldest puzzles in molecular biology—that of the divergent observations of fully discontinuous leading-strand replication in vivo versus continuous replication in vitro (22, 67). Employing the classical techniques of alkaline sucrose-gradient sedimentation and Southern hybridization, in tandem with a unique pH-neutral denaturing gradient system, we revealed the nearly continuous replication of the leading strand in *E. coli*. This highly continuous in vivo replication was observed only in excision repair-deficient mutants, and ribonucleotide excision repair was identified as the major driver of leading-strand scission. Pulsed-labeled RIs from the *lig ZER ΔB* strain, which lacks all known pathways for excision repair, appeared as two distinct populations of either LMW (0.5- to 5-kb) Okazaki fragments or HMW (20- to 300-kb) pieces, the latter being similar in size to the chronically labeled chromosomal DNA (Fig. 2*C*). Strand-specific hybridization of these nascent DNA strands revealed a leading-strand origin for HMW RIs, while the LMW RIs were mostly derived from the lagging strand. Comparisons of LMW and HMW specificity ratios (Fig. 4*B*) indicate a relative lead/lag ratio enrichment factor of nearly 80-fold between the fractions. Control hybridization experiments suggest that the observed enrichment factor approaches the maximum possible for this assay in its current form (*SI Appendix*, Figs. S7 and S8). Therefore, it appears that, save for the occasional repriming, the leading strand is synthesized by a nearly continuous mechanism, only to become fragmented by excision repair soon after replication-fork passage. In other words, newly synthesized DNA is quite "dirty," being initially synthesized with a significant number of chemically incorrect bases, mostly ribonucleotides, and undergoes significant excision repair before its maturation into chromosomal DNA. Since the size of LMW RIs is unaltered by the inactivation of excision-repair systems, the LMW population likely constitutes bona fide RNA-primed Okazaki fragments.

As excision repair must be inhibited to produce a more continuous leading strand, inactivation of only a subset of repair systems allows for determination of the contribution of individual repair pathways to the overall RI fragmentation. While our study lacked granularity regarding DNA-only excision repair, we did examine the contribution of ribonucleotide excision repair to leading-strand fragmentation. Tests for the individual contributions of mono-rN and DNA excision activities revealed that RNase HII cleaves the leading strand at a frequency similar to the combined effects of all other excision-repair systems (Fig. 3 *B* and *D*). Supporting this result, our in vitro data indicate a mono-rN density in the DNA of *rnhB* mutants of one in 8,000 to 9,000 nt (Fig. 1 *D*–*F*). Therefore, excision-proficient cells produce LMW RIs that are a mixture of lagging-strand Okazaki fragments and excision-fragmented leading strands. However, these leading- and lagging-strand fragment populations are not entirely overlapping; hybridization of the "shoulder" population from an excision-proficient strain displayed a clear leading-strand bias, whereas the classic Okazaki peak was mostly lagging-strand in origin (Fig. 4*A*). As such, our results for the repair-proficient *ligA*(Ts) strain closely mirror those obtained by Louarn and Bird during their isolation and hybridization of RIs from *polA*(Ts) mutant cells (27).

Is leading-strand replication completely continuous in vivo, as depicted in textbooks? Our data suggest that it is not. When we pulsed ligase-deficient cells for shorter periods than normal (Fig. 6*B*), the leading-strand fragments steadily decreased in size with shorter pulses. If the leading-strand synthesis were primed only once at the origin, as implied in some replication models (68), then no more than 1% of asynchronously dividing *E. coli* cells would possess leading strands shorter than 50 kb, irrespective of pulse length. Since pulse-length invariance is not observed, leading-strand repriming events occur with a minimum periodicity of 50 to

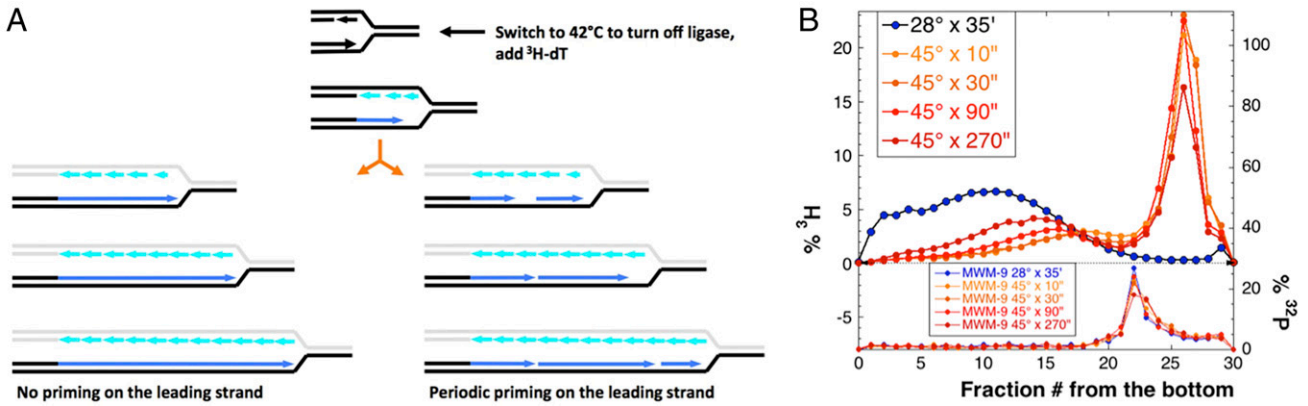

Fig. 6. Evidence for periodic priming on the leading strand. (*A*) If the leading strands were replicated continuously, with no regular repriming events (*Left*), incorporation of [^{3}H]thymidine into the nascent leading strands is expected to produce tritiated HMW species whose length is independent of the labeling pulse time (since nascent DNA is always attached to the rest of the chromosome). On the other hand, if the leading strands were replicated in smaller subchromosome-sized fragments (*Right*), shorter pulses would reduce the apparent size of nascent leading-strand fragments. (*B*) AS gradient of the *lig ZER ΔB* mutant (eGC197), either labeled chronically (28 °C × 35 min) for full-length chromosomal DNA or pulse labeled at 45 °C for 10, 30, 90, or 270 s to label RIs.

70 kb. It is of course possible that leading-strand synthesis is more continuous than seen here, and that as-yet unrecognized excision-repair activities impart a low-level residual fragmentation.

That leading-strand repriming catalyzes the bypass of fork-blocking lesions in template DNA was demonstrated 50 y ago for UV-induced pyrimidine dimers (69). While the mechanisms underlying leading-strand repriming in vivo remain unexplored, direct bypass of pyrimidine dimers by a primase-dependent pathway has been demonstrated in vitro (70, 71), where blocking extension by the leading-strand polymerase slowed helicase progression until repriming could occur on the accumulating ssDNA of the leading-strand template. This scenario is especially relevant for our experimental system, as some fork-blocking lesions may accumulate in the *lig ZER ΔB* multiple excision-repair strain, used here to detect HMW RIs, resulting in a higher frequency of leading-strand repriming.

In general, leading-strand repriming assumes specific inhibition of the leading-strand polymerase relative to the replicative helicase, to generate ssDNA on the leading-strand template. Besides blocking DNA lesions, other potential replication irregularities may cause leading-strand repriming, such as incorporation of chain-terminating base analogs such as azidothymidine (72), or malfunctioning replisomes [for example, in *holC* and *holD* mutants (73)] or depletion of a specific DNA precursor, as during thymine starvation (74). Finally, although not observed in vitro, a regular, damage-independent leading-strand repriming, as first hypothesized by Okazaki et al. (11), could function similar to the "clock"-type mechanism of helicase-primase binding for lagging-strand priming (75), perhaps at a greatly reduced cadence. Another primase-independent pathway has also been demonstrated in vitro (76), according to which the replisome recruits nascent mRNA to directly reprime the leading strand after collision with, and displacement of, a codirectional transcription-elongation complex.

In summary, this work unifies 50 y of incongruent in vivo and in vitro results concerning the continuity of leading-strand replication, by showing that in vivo demonstrations of Okazaki fragment formation on the leading strand were the result of fragmentation of nascent strands by excision DNA repair. Although this fragmentation was long-suspected, a definitive demonstration of continuous leading-strand replication in the absence of repair activities had remained elusive (22). It now appears that in vivo nascent DNA contains at a minimum 1 incorrect base per ~10,000 nt synthesized, with most of these "wrong" bases consisting of ribonucleotides. That in vitro replication assays have generally failed to observe leading-strand discontinuities is likely due to the omission from replication reactions of nucleotide contaminants and their cognate excision enzymes. Indeed, it now appears highly unlikely that *E. coli* leading strands exhibit the level of continuity seen in vitro, where leading-strand length can exceed one-quarter of a megabase (77). However, in vitro studies addressing the mechanisms of base misincorporation, lesion bypass, and replication restart are coming to the fore (78). The in vivo methods presented here produce a clean separation of bona fide lagging-strand Okazaki fragments from the mostly continuous leading strands, and so offer a new avenue for the study of strand-specific effects of mutations or conditions perturbing replication. The nature and frequency of periodic leading-strand repriming are the next questions to answer.

Materials and Methods

Bacterial strains and plasmids are described in *SI Appendix* and in *SI Appendix*, Table S1.

Growth Conditions, Radiolabeling, Stop Solution, and DNA Isolation. Strains were grown at 28 °C, either in LB (10 g tryptone, 5 g yeast extract, 5 g NaCl/L, pH 7.2 with NaOH) or on LB plates (15 g agar/L of LB broth). Incubation of liquid cultures was performed in appropriately sized vessels and with sufficient shaking to effect robust aerobic growth. For labeling experiments, a single colony was grown overnight at 28 °C to saturation in LB and diluted 30 to 100× into 5 mL of LB in the morning. The starting OD_{600} of subcultures was *lig* and *lig ΔB* OD 0.02, *lig ZER* OD 0.05, and *lig ZER ΔB* OD 0.06. Subcultures were grown at 28 °C for ~3.5 h to OD ~0.5 to 0.6 and labeled by addition of 5 to 10 μCi/mL of 60 to 90 Ci/mmol [^{3}H]thymidine (PerkinElmer). We found that growing strains past an OD of 0.4 in LB allowed for much increased thymidine incorporation (*SI Appendix*, Fig. S3), likely due to exhaustion of dT in LB. Bulk chromosomal DNA was labeled at 28 °C for 35 min. To pulse label replication intermediates, we shifted 5 mL of culture to 42 °C for 4 min before adding label and incubating for an additional 2 min. Labeling was stopped by mixing the culture with the stopping solution [five volumes of 10 mM KCN, 10% pyridine (79), kept on ice throughout the experiment]. Direct comparison of this ice-cold KCN/pyridine mixture with the phenol-ethanol-acetate stopping solution (80), used by Okazaki (15) and by us before (30, 31), showed no difference in RI distribution, but we found cell pellets stopped with KCN/pyridine were easier to resuspend before lysis. Once mixed with the stopping solution, cells were pelleted, and the pellets were resuspended in 1 mL of 30% sucrose, 50 mM Tris (pH 8.0), moved to Eppendorf tubes, and again pelleted at 13,000 × *g* for 2 min. Pellets were then resuspended in 50 μL of the same buffered 30% sucrose and lysed by addition of 350 μL of 2% SDS, 40 mM EDTA, 50 mM Tris (pH 8.0) and incubation at 65 °C for 5 min. Lysates were sequentially extracted with equal volumes of phenol (pH 8), 50:50 phenol/chloroform, and chloroform (*SI Appendix*, Fig. S2). The aqueous phase was moved to DNA LoBind microcentrifuge tubes (Eppendorf) and precipitated twice with ethanol in the

presence of 150 mM KCl. The final DNA pellet was resuspended in 100 μL of TE buffer (10 mM Tris HCl pH 8.0, 1 mM EDTA).

Plasmid Assay for RNA Density and Alkaline-Liable Sites. Assays of RNase HII sensitivity and alkali sensitivity of plasmid DNA were performed as described previously (52), but the plasmid was pCY566 (81). For linear plasmid species treated with formamide or NaOH, the average number of strand breaks was derived from the zero class of the Poisson distribution, taking into account the background level of nicks in parental molecules (82), by the equation $-\ln(F_{treated}/F_{untreated})$, where $F_{treated}$ is the fraction of the full-length ssDNA in 0.3 M NaOH, 45 °C × 90-min treatment, and $F_{untreated}$ is the fraction of the full-length ssDNA in 0.2 M NaOH, 0 °C × 5-min treatment or dissolution in 100% formamide. The average density of the nicks was determined by dividing the total single-stranded plasmid length in nucleotides by the average number of nicks per molecule.

Alkaline-Sucrose Gradients. Alkaline-sucrose gradients were made essentially as described (15). Briefly, 15.6-mL linear gradients of 5 to 20% sucrose in 0.1 M NaOH, 0.9 M NaCl, 1 mM EDTA were formed in 16 × 102-mm polypropylene ultracentrifuge tubes (Beckman; 337986) using an SG15 gradient maker (Hoefer). Gradients were poured from the bottom up by pumping the solution at ∼1.5 mL/min through a length of tubing capped with a glass capillary tube. During pouring, just as the final 20% of solution exited the mixing chamber, flow was stopped, and a 1.2-mL shelf of 80% sucrose, in the same buffer, was added and pumped to the bottom of the tube. Finished gradients were balanced and chilled at 4 °C for at least 1 h before loading. Our DNA-treatment protocol includes, for historical reasons, a mock alkali treatment step: To each 100-μL DNA solution was added 100 μL of 0.6 M NaCl, and the mixture was incubated at 45 °C for 1 h. Following this mock treatment, a few microliters of [^{32}P]marker DNA was added, and the mixture was chilled in an ice/water bath for 20 min. To denature the DNA, 200 μL of ice-cold 0.4 M NaOH was added and the mixture was maintained on ice for 20 min. The centrifuge, rotor, and buckets were all precooled to 4 °C. Denatured DNA samples were slowly pipetted onto the gradients. If phage DNA was included, it was liberated from concentrated phage particle stocks (>10^{12} PFU/mL) by mixing a small volume (1 to 4 μL) with an equal volume of 0.4 M Na_3PO_4 (55, 83) on a spoon-type spatula and then layering this mixture on top of the sample layer. Gradients were centrifuged in a Beckman SW28.1 Ti rotor at 19,000 rpm for 20 h at 4 °C. For fractionation, the centrifuge tube was immobilized on a makeshift stand, and its bottom was punctured with a 32-gauge needle. Fractions were collected through the needle, with the flow rate controlled by a peristaltic pump connected to the top of the tube by a stopper. It took ∼20 min to fractionate each 16.8-mL gradient into 29 fractions of ∼550 μL. Fifty to 100 μL of each fraction was added directly to 4 mL of Bio-Safe II scintillation fluid (RPI) and counted in a liquid scintillation counter. Fraction zero, representing tritiated DNA that had penetrated the 80% sucrose cushion, was obtained by rinsing the empty centrifuge tube twice with 100% ethanol, removing the tube bottom with scissors, and placing it in a tube with scintillant. To identify the position of lambda or T4 phage DNA in a gradient, 200 μL of each fraction was dot blotted to a nylon membrane and hybridized with a phage-specific probe using standard methods (84).

Formamide-Urea-Sucrose Gradients. Pouring, fractionation, scintillation counting, and phage-marker hybridization procedures were identical to those detailed for alkaline sucrose. Formamide was from Fisher (99%, molecular biology grade), and anhydrous urea was from Sigma (≥99%, ACS grade). Formamide, if not freshly opened, was deionized immediately before use by stirring for 1 h with 5% (wt/vol) bed-bed ion-exchange resin [Bio-Rex MSZ-501(D); Bio-Rad] (85). Linear 16.4-mL 5 to 40% sucrose gradients, without a shelf, were formed in 70% formamide, 1 M urea, 1 M NaCl, 10 mM Tris (pH 7.5), 1 mM EDTA. Samples were prepared as for alkaline sucrose but, after mock alkali treatment, 50 μL of 100 mM Tris (pH 7.5) was added to each DNA sample, to bring the total volume to 250 μL. Two hundred and fifty microliters of 99% formamide was then added, followed by 360 mg of dry urea, and the samples were gently rocked to dissolve the urea. [^{32}P]marker DNA and phage particles were added and dispersed by gentle inversion. Just before loading, DNA solutions were denatured by incubation at 80 °C for 20 min and immediately but slowly pipetted onto the gradients that were kept at 4 °C, and centrifuged in a Beckman SW28.1 Ti rotor at 20,500 rpm for 44 h at 4 °C.

ssRNA Preparation and Strand-Specific Hybridization. The two pGEM-4::*gspD-M* plasmids described above, which contain the *gsp* operon in either of the two orientations, were linearized with BamHI for use as templates for production of 8.8-kb stand-specific ssRNAs using an AmpliScribe T7-Flash Kit (Epicenter) according to the manufacturer's instructions. For hybridization, ssRNAs were denatured in formamide/formaldehyde as described (84), and applied to Hybond-XL nylon membrane (GE Healthcare) in 3-mm-diameter circles using a dot-blot vacuum manifold (Bio-Rad). Twenty micrograms of ssRNA (*SI Appendix*, Fig. S7) was applied per spot and immobilized by UV cross-linking (UVP Scientific). Membranes were cut into 8 × 16-mm pieces containing individual spots of RNA and placed singly into screwcap 1.5-mL microcentrifuge tubes. One milliliter of hybridization buffer (8% SDS, 0.5 M $NaPO_4$, 10 mM EDTA, pH 7.2) was added and the tubes were rotated end over end at 55 °C for at least 1 h. Gradient fractions for hybridization were pooled and concentrated to 200 μL in TE buffer by centrifugal dialysis (Amicon Ultra-4, 10K NMWL; Millipore). Dialysates were moved to screwcap Eppendorf tubes and sonicated (*SI Appendix*, Fig. S6) at 75% power, 100% duty cycle, in the "cup horn" attachment of a Misonix S-4000 sonicator chilled to 4 °C, and then brought to a total volume of 1.5 mL in 1× hybridization buffer. Hybridization mixtures were boiled for 5 min and kept at 65 °C before each was split into two tubes containing the membrane-attached Watson or Crick *gsp* ssRNA targets. Hybridization proceeded overnight at 55 °C, after which membranes were removed to trays and washed successively for 30-min intervals with 5 mL each of 2× SSC, 0.5× SSC, and 0.1× SSC, each containing 0.5% SDS. To improve the efficiency of tritium counting, membranes were moved to fresh screwcap Eppendorf tubes and stripped by boiling in 250 μL of 0.2 M NaOH. Stripping solution was then neutralized by addition of 250 μL of 0.2 M acetic acid, 100 mM Tris (pH 7.5), added to 4 mL of scintillation fluid (Bio-Safe II; RPI), and counted to 2% error in a liquid scintillation counter.

ACKNOWLEDGMENTS. We thank Stuart Shuman (Sloan-Kettering Institute) for reminding us of the importance of *rnhB* inactivation for the quest to understand the nature of RIs in ligase-deficient conditions, and Luciana Amado Bustamante (Universidad Peruana de Ciencias) for critical reading of the manuscript. We are grateful to John E. Cronan for encouraging the development of this project and for helpful discussions on alternative sucrose-gradient solvents. We are grateful to all members of the A.K. laboratory for their enthusiastic support of this project. This work was supported by National Institutes of Health Grant GM 073115.

1. Watson JD, Crick FHC (1953) Molecular structure of nucleic acids; a structure for deoxyribose nucleic acid. *Nature* 171:737–738.
2. Shchyolkina AK, et al. (2000) Parallel-stranded DNA with mixed AT/GC composition: Role of trans G·C base pairs in sequence dependent helical stability. *Biochemistry* 39:10034–10044.
3. Levinthal C, Crane HR (1956) On the unwinding of DNA. *Proc Natl Acad Sci USA* 42:436–438.
4. Freese E (1958) The arrangement of DNA in the chromosome. *Cold Spring Harb Symp Quant Biol* 23:13–18.
5. Cairns J (1963) The chromosome of *Escherichia coli*. *Cold Spring Harbor Symp Quant Biol* 28:43–46.
6. Cairns J (1963) The bacterial chromosome and its manner of replication as seen by autoradiography. *J Mol Biol* 6:208–213.
7. Okazaki T, Okazaki R (1969) Mechanism of DNA chain growth. IV. Direction of synthesis of T4 short DNA chains as revealed by exonucleolytic degradation. *Proc Natl Acad Sci USA* 64:1242–1248.
8. Kornberg A (1974) *DNA Synthesis* (W.H. Freeman, San Francisco).
9. Gefter ML, Molineux IJ, Kornberg T, Khorana HG (1972) Deoxyribonucleic acid synthesis in cell-free extracts. 3. Catalytic properties of deoxyribonucleic acid polymerase II. *J Biol Chem* 247:3321–3326.
10. Kornberg T, Gefter ML (1972) Deoxyribonucleic acid synthesis in cell-free extracts. IV. Purification and catalytic properties of deoxyribonucleic acid polymerase III. *J Biol Chem* 247:5369–5375.
11. Okazaki R, Okazaki T, Sakabe K, Sugimoto K, Sugino A (1968) Mechanism of DNA chain growth. I. Possible discontinuity and unusual secondary structure of newly synthesized chains. *Proc Natl Acad Sci USA* 59:598–605.
12. Yudelevich A, Ginsberg B, Hurwitz J (1968) Discontinuous synthesis of DNA during replication. *Proc Natl Acad Sci USA* 61:1129–1136.
13. Okazaki R, et al. (1968) In vivo mechanism of DNA chain growth. *Cold Spring Harb Symp Quant Biol* 33:129–143.
14. Bird RE, Lark KG (1970) Chromosome replication in *Escherichia coli* 15T$^-$ at different growth rates: Rate of replication of the chromosome and the rate of formation of small pieces. *J Mol Biol* 49:343–366.
15. Okazaki R (1974) Short-chain intermediates. *DNA Replication, Methods in Molecular Biology*, ed Wickner RB (Marcel Dekker, New York), Vol 7, pp 1–32.
16. Okazaki R, Arisawa M, Sugino A (1971) Slow joining of newly replicated DNA chains in DNA polymerase I-deficient *Escherichia coli* mutants. *Proc Natl Acad Sci USA* 68: 2954–2957.
17. Sugimoto K, Okazaki T, Imae Y, Okazaki R (1969) Mechanism of DNA chain growth. 3. Equal annealing of T4 nascent short DNA chains with the separated complementary strands of the phage DNA. *Proc Natl Acad Sci USA* 63:1343–1350.
18. Sugimoto K, Okazaki T, Okazaki R (1968) Mechanism of DNA chain growth, II. Accumulation of newly synthesized short chains in *E. coli* infected with ligase-defective T4 phages. *Proc Natl Acad Sci USA* 60:1356–1362.

19. Sakabe K, Okazaki R (1966) A unique property of the replicating region of chromosomal DNA. *Biochim Biophys Acta* 129:651–654.
20. Kurosawa Y, Okazaki R (1975) Mechanism of DNA chain growth. XIII. Evidence for discontinuous replication of both strands of P2 phage DNA. *J Mol Biol* 94:229–241.
21. Pauling C, Hamm L (1969) Properties of a temperature-sensitive, radiation-sensitive mutant of *Escherichia coli*. II. DNA replication. *Proc Natl Acad Sci USA* 64:1195–1202.
22. Okazaki T (2017) Days weaving the lagging strand synthesis of DNA—A personal recollection of the discovery of Okazaki fragments and studies on discontinuous replication mechanism. *Proc Jpn Acad Ser B Phys Biol Sci* 93:322–338.
23. Nuzzo F, Brega A, Falaschi A (1970) DNA replication in mammalian cells. I. The size of newly synthesized helices. *Proc Natl Acad Sci USA* 65:1017–1024.
24. Horwitz MS (1971) Intermediates in the synthesis of type 2 adenovirus deoxyribonucleic acid. *J Virol* 8:675–683.
25. Gautschi JR, Clarkson JM (1975) Discontinuous DNA replication in mouse P-815 cells. *Eur J Biochem* 50:403–412.
26. Dermody JJ, Robinson GT, Sternglanz R (1979) Conditional-lethal deoxyribonucleic acid ligase mutant of *Escherichia coli*. *J Bacteriol* 139:701–704.
27. Louarn J-M, Bird RE (1974) Size distribution and molecular polarity of newly replicated DNA in *Escherichia coli*. *Proc Natl Acad Sci USA* 71:329–333.
28. Nasmyth KA (1977) Temperature-sensitive lethal mutants in the structural gene for DNA ligase in the yeast *Schizosaccharomyces pombe*. *Cell* 12:1109–1120.
29. Johnston LH, Nasmyth KA (1978) *Saccharomyces cerevisiae* cell cycle mutant *cdc9* is defective in DNA ligase. *Nature* 274:891–893.
30. Amado L, Kuzminov A (2006) The replication intermediates in *Escherichia coli* are not the product of DNA processing or uracil excision. *J Biol Chem* 281:22635–22646.
31. Amado L, Kuzminov A (2013) Low-molecular-weight DNA replication intermediates in *Escherichia coli*: Mechanism of formation and strand specificity. *J Mol Biol* 425: 4177–4191.
32. Konrad EB, Modrich P, Lehman IR (1974) DNA synthesis in strains of *Escherichia coli* K12 with temperature-sensitive DNA ligase and DNA polymerase I. *J Mol Biol* 90: 115–126.
33. Wang T-CV, Chen S-H (1994) Okazaki DNA fragments contain equal amounts of lagging-strand and leading-strand sequences. *Biochem Biophys Res Commun* 198: 844–849.
34. Wang T-CV, Smith KC (1989) Discontinuous DNA replication in a *lig-7* strain of *Escherichia coli* is not the result of mismatch repair, nucleotide-excision repair, or the base-excision repair of DNA uracil. *Biochem Biophys Res Commun* 165:685–688.
35. Bradshaw JS, Kuzminov A (2003) RdgB acts to avoid chromosome fragmentation in *Escherichia coli*. *Mol Microbiol* 48:1711–1725.
36. Budke B, Kuzminov A (2010) Production of clastogenic DNA precursors by the nucleotide metabolism in *Escherichia coli*. *Mol Microbiol* 75:230–245.
37. Tye B-K, Lehman IR (1977) Excision repair of uracil incorporated in DNA as a result of a defect in dUTPase. *J Mol Biol* 117:293–306.
38. Tye BK, Nyman PO, Lehman IR, Hochhauser S, Weiss B (1977) Transient accumulation of Okazaki fragments as a result of uracil incorporation into nascent DNA. *Proc Natl Acad Sci USA* 74:154–157.
39. Olivera BM (1978) DNA intermediates at the *Escherichia coli* replication fork: Effect of dUTP. *Proc Natl Acad Sci USA* 75:238–242.
40. Olivera BM, Manlapaz-Ramos P, Warner HR, Duncan BK (1979) DNA intermediates at the *Escherichia coli* replication fork. II. Studies using dut and ung mutants in vitro. *J Mol Biol* 128:265–275.
41. Tamanoi F, Okazaki T (1978) Uracil incorporation into nascent DNA of thymine-requiring mutant of *Bacillus subtilis* 168. *Proc Natl Acad Sci USA* 75:2195–2199.
42. Tamanoi F, Machida Y, Okazaki T (1979) Uracil incorporation into nascent DNA of *Bacillus subtilis* and *Escherichia coli*. *Cold Spring Harb Symp Quant Biol* 43:239–242.
43. Tye B-K, Chien J, Lehman IR, Duncan BK, Warner HR (1978) Uracil incorporation: A source of pulse-labeled DNA fragments in the replication of the *Escherichia coli* chromosome. *Proc Natl Acad Sci USA* 75:233–237.
44. Cha TA, Alberts BM (1989) The bacteriophage T4 DNA replication fork. Only DNA helicase is required for leading strand DNA synthesis by the DNA polymerase holoenzyme. *J Biol Chem* 264:12220–12225.
45. Nakai H, Richardson CC (1988) Leading and lagging strand synthesis at the replication fork of bacteriophage T7. Distinct properties of T7 gene *4* protein as a helicase and primase. *J Biol Chem* 263:9818–9830.
46. Wu CA, Zechner EL, Marians KJ (1992) Coordinated leading- and lagging-strand synthesis at the *Escherichia coli* DNA replication fork. I. Multiple effectors act to modulate Okazaki fragment size. *J Biol Chem* 267:4030–4044.
47. Kornberg A (1980) *DNA Replication* (W.H. Freeman, San Francisco).
48. Machida Y, Okazaki T, Miyake T, Ohtsuka E, Ikehara M (1981) Characterization of nascent DNA fragments produced by excision of uracil residues in DNA. *Nucleic Acids Res* 9:4755–4766.
49. Williams JS, Kunkel TA (2014) Ribonucleotides in DNA: Origins, repair and consequences. *DNA Repair (Amst)* 19:27–37.
50. Williams JS, Lujan SA, Kunkel TA (2016) Processing ribonucleotides incorporated during eukaryotic DNA replication. *Nat Rev Mol Cell Biol* 17:350–363.
51. Yao NY, Schroeder JW, Yurieva O, Simmons LA, O'Donnell ME (2013) Cost of rNTP/dNTP pool imbalance at the replication fork. *Proc Natl Acad Sci USA* 110: 12942–12947.
52. Kouzminova EA, Kadyrov FF, Kuzminov A (2017) RNase HII saves *rnhA* mutant *Escherichia coli* from R-loop-associated chromosomal fragmentation. *J Mol Biol* 429: 2873–2894.
53. Tamm C, Shapiro HS, Lipshitz R, Chargaff E (1953) Distribution density of nucleotides within a desoxyribonucleic acid chain. *J Biol Chem* 203:673–688.
54. Kouzminova EA, Kuzminov A (2012) Chromosome demise in the wake of ligase-deficient replication. *Mol Microbiol* 84:1079–1096.
55. Abelson J, Thomas CA (1966) The anatomy of the T5 bacteriophage DNA molecule. *J Mol Biol* 18:262–288.
56. Marmur J, Ts'o PO (1961) Denaturation of deoxyribonucleic acid by formamide. *Biochim Biophys Acta* 51:32–36.
57. Chomczynski P (1992) Solubilization in formamide protects RNA from degradation. *Nucleic Acids Res* 20:3791–3792.
58. Hegedüs E, Kókai E, Kotlyar A, Dombrádi V, Szabó G (2009) Separation of 1–23-kb complementary DNA strands by urea-agarose gel electrophoresis. *Nucleic Acids Res* 37:e112.
59. Bouché JP, Zechel K, Kornberg A (1975) *dnaG* gene product, a rifampicin-resistant RNA polymerase, initiates the conversion of a single-stranded coliphage DNA to its duplex replicative form. *J Biol Chem* 250:5995–6001.
60. Sternglanz R, Wang HF, Donegan JJ (1976) Evidence that both growing DNA chains at a replication fork are synthesized discontinuously. *Biochemistry* 15:1838–1843.
61. Kuzminov A (2014) The precarious prokaryotic chromosome. *J Bacteriol* 196: 1793–1806.
62. Dunn AR, Hassell JA (1977) A novel method to map transcripts: Evidence for homology between an adenovirus mRNA and discrete multiple regions of the viral genome. *Cell* 12:23–36.
63. Francetic O, Belin D, Badaut C, Pugsley AP (2000) Expression of the endogenous type II secretion pathway in *Escherichia coli* leads to chitinase secretion. *EMBO J* 19: 6697–6703.
64. Low B (1968) Formation of merodiploids in matings with a class of Rec- recipient strains of *Escherichia coli* K12. *Proc Natl Acad Sci USA* 60:160–167.
65. Van Dyk TK, Gatenby AA, LaRossa RA (1989) Demonstration by genetic suppression of interaction of GroE products with many proteins. *Nature* 342:451–453.
66. Tokuriki N, Tawfik DS (2009) Chaperonin overexpression promotes genetic variation and enzyme evolution. *Nature* 459:668–673.
67. Wang TC (2005) Discontinuous or semi-discontinuous DNA replication in *Escherichia coli*? *BioEssays* 27:633–636.
68. Baker TA, Wickner SH (1992) Genetics and enzymology of DNA replication in *Escherichia coli*. *Annu Rev Genet* 26:447–477.
69. Rupp WD, Howard-Flanders P (1968) Discontinuities in the DNA synthesized in an excision-defective strain of *Escherichia coli* following ultraviolet irradiation. *J Mol Biol* 31:291–304.
70. Heller RC, Marians KJ (2006) Replication fork reactivation downstream of a blocked nascent leading strand. *Nature* 439:557–562.
71. Yeeles JT, Marians KJ (2013) Dynamics of leading-strand lesion skipping by the replisome. *Mol Cell* 52:855–865.
72. Cooper DL, Lovett ST (2011) Toxicity and tolerance mechanisms for azidothymidine, a replication gap-promoting agent, in *Escherichia coli*. *DNA Repair (Amst)* 10:260–270.
73. Duigou S, Silvain M, Viguera E, Michel B (2014) ssb gene duplication restores the viability of Δ*holC* and Δ*holD Escherichia coli* mutants. *PLoS Genet* 10:e1004719.
74. Kuong KJ, Kuzminov A (2012) Disintegration of nascent replication bubbles during thymine starvation triggers RecA- and RecBCD-dependent replication origin destruction. *J Biol Chem* 287:23958–23970.
75. Tougu K, Marians KJ (1996) The interaction between helicase and primase sets the replication fork clock. *J Biol Chem* 271:21398–21405.
76. Pomerantz RT, O'Donnell M (2008) The replisome uses mRNA as a primer after colliding with RNA polymerase. *Nature* 456:762–766.
77. Graham JE, Marians KJ, Kowalczykowski SC (2017) Independent and stochastic action of DNA polymerases in the replisome. *Cell* 169:1201–1213.e17.
78. Marians KJ (2018) Lesion bypass and the reactivation of stalled replication forks. *Annu Rev Biochem* 87:217–238.
79. Jacobson MK, Lark KG (1973) DNA replication in *Escherichia coli*: Evidence for two classes of small deoxyribonucleotide chains. *J Mol Biol* 73:371–396.
80. Manor H, Goodman D, Stent GS (1969) RNA chain growth rates in *Escherichia coli*. *J Mol Biol* 39:1–29.
81. Cronan JE (2013) Improved plasmid-based system for fully regulated off-to-on gene expression in *Escherichia coli*: Application to production of toxic proteins. *Plasmid* 69: 81–89.
82. Kouzminova EA, Kuzminov A (2006) Fragmentation of replicating chromosomes triggered by uracil in DNA. *J Mol Biol* 355:20–33.
83. Freifelder D, Davison PF (1963) Physicochemical studies on the reaction between formaldehyde and DNA. *Biophys J* 3:49–63.
84. Sambrook J, Fritsch EF, Maniatis T (1989) *Molecular Cloning: A Laboratory Manual* (Cold Spring Harbor Lab Press, Cold Spring Harbor, NY).
85. Samanta HK, Engel D (1987) Deionization of formamide with Biorad AG501-X(D). *J Biochem Biophys Methods* 14:261–266.